Bio-inspired design and dynamic maneuverability of a minimally actuated six-legged robot

Aaron M. Hoover †, Samuel Burden‡, Xiao-Yu Fu*, S. Shankar Sastry‡, and R. S. Fearing‡

***Abstract*— Rapidly running arthropods like cockroaches make use of passive dynamics to achieve remarkable locomotion performance with regard to stability, speed, and maneuverability. In this work, we take inspiration from these organisms to design, fabricate, and control a 10cm, 24 gram underactuated hexapedal robot capable of running at 14 body lengths per second and performing dynamic turning maneuvers. Our design relies on parallel kinematic mechanisms fabricated using the scaled smart composite microstructures (SCM) process and viscoelastic polymer legs with tunable stiffness. In addition to the novel robot design, we present experimental validation of the lateral leg spring (LLS) locomotion model's prediction that dynamic turning can be achieved by modulating leg stiffness. Finally, we present and validate a leg design for active stiffness control using shape memory alloy and demonstrate the ability of the robot to execute near-gymnastic 90° turns in the span of five strides.**

I. Introduction

For organisms, dynamic mechanically-mediated stability is the norm [10]. The American cockroach *Periplaneta americana* runs at 50 body lengths per second while relying primarily on feedforward clock-driven control [9]. Entire families of dynamic maneuvers can be built upon the same basic gait simply by modulating force production with slight adjustments to timing and posture [16], [26]. Further, dynamic legged locomotion can confer stability even when energy is conserved [29], partially explaining why the cockroach *Blaberus discoidalis* can traverse highly fractured terrain without significantly altering neural activation patterns in its propulsion muscles [31] and can rapidly recover from a substantial lateral perturbation while running at full speed [15]. Inspired by the principles underlying these remarkable examples of effective locomotion, we hypothesize that embracing passive mechanical self-stabilization will enable us to build high-performing small-scale legged robots.

Small scale mobile robots—those with masses on the order of grams and dimensions on the order of single centimeters—possess myriad advantages compared to their larger counterparts. Small size enables them to operate in environments where large robots would be impractical and, at a few dollars per robot, large quantities may be manufactured affordably [14]. In addition, the ratio of surface area to volume (and therefore mass) is relatively high for small robots. This can engender striking physical resilience on par with some of nature's sturdiest arthropods, for example enabling a small legged robot to survive a collision with the ground at its terminal velocity [6].

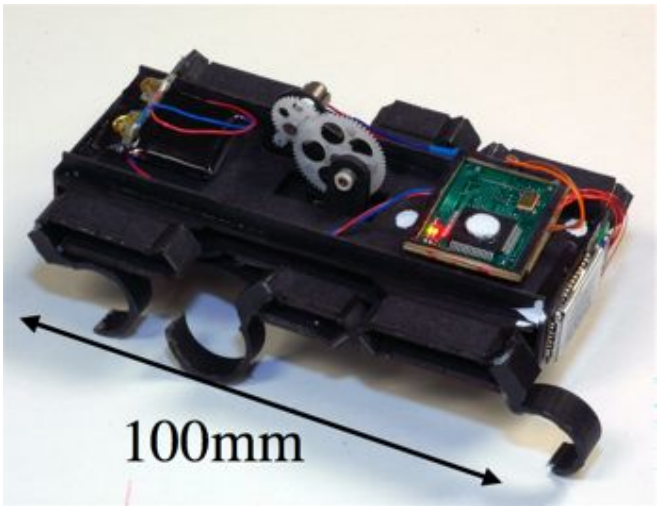

Fig. 1: The DynaRoACH robot.

Unfortunately, the design and construction of small mobile robots is currently quite challenging. Design at small scales necessitates tight coupling between structural kinematics, dynamics, actuation, and control [3]. Stringent weight constraints restrict the feasible numbers and sizes of actuators, hence uncontrolled degrees of freedom are unavoidable and novel fabrication approaches [33] are typically required. Limitations on power density impose a trade-off between locomotion and computation; achieving rapid motion restricts the allowed complexity of onboard control algorithms. Taken together, these constraints necessitate increased reliance on passive mechanical control for these robots.

Biology has strongly influenced the development of high performance legged locomotors. An early example of a robust, dynamic, many-legged robot is RHex [27], which was explicitly designed to instantiate a low-dimensional dynamical abstraction of running. More recently, robots like Sprawlita [8], Mini-Whegs [24], and iSprawl [18] have pushed the performance boundaries of dynamic locomotion. A newly-developed dynamic hexapedal robot, DASH [6], is steerable and capable of running at 15 body lengths per second while weighing only 16 grams. Despite the impressive performance of these legged robots in straight-ahead movement, dynamic maneuvers remain elusive. The role of passive dynamics in robotic somersaults have been

The work was supported by the Army Research Laboratory under the Micro Autonomous Systems and Technology Collaborative Technology Alliance.

Corresponding author: ahoover@eecs.berkeley.edu, † Dept. of Mechanical Engineering, University of California, Berkeley

‡ Dept. of Electrical Engineering and Computer Science, University of California, Berkeley

∗ Dept. of Bioengineering, University of California, Berkeley

studied in bipeds [25], [13], and some recent work has resulted in small-scale jumping robots [19], [4].

In this work, we present the kinematic design of a lightweight and efficient compliant transmission capable of driving a small legged robot from a single motor. The single motor design drastically reduces the mass of the robot and yields a feedforward clock-driven gait. Coupling the transmission with passive compliant legs which exhibit viscoelastic damping results in stable dynamic straight-ahead running. Inspired by turning mechanisms in cockroaches, we demonstrate the potential to achieve turning during dynamic running by varying the stiffness of a single leg. For this work, stiffness was adjusted by physically exchanging the nominal legs for those fabricated from a stiffer material. We also experimentally establish the feasibility of using shape memory alloy wire to actively induce a change in the dynamic stiffness of the leg, providing a path to integration. Finally, preliminary data suggest that a large change in stiffness may enable dynamic maneuvers such as full-speed 90° turns over the course of 5 strides.

II. Robot Design

A major challenge in building a small-scale light-weight many-legged robot is the minimization of the number of actuators required to produce effective locomotion. The primary gait used by cockroaches running at high speed is the alternating tripod gait in which ipsilateral front and hind legs move in phase with the contralateral middle leg. Inspired by the incredible locomotory performance of these animals, we sought to design a robot's kinematics such that all six legs could be driven by a single actuator to produce the alternating tripod gait at high speeds. Though it may seem arbitrary to restrict ourselves to a single motor for forward running, a minimal number of actuators is generally desirable for small-scale robots due to constraints on power density. In fact, for legged robot designs employing one motor per leg, each motor only does positive work on the robot for approximately 30% of the stride.

We have chosen a brushed DC motor as our primary power actuator. DC motors have a variety of advantages; they are: relatively power dense [32]; inexpensive; straightforward to control; and commercially available in a variety of windings, yielding a range of torque and speed characteristics. However, due to the small size of the motor and therefore high operating speed, we employ a large gear reduction of approximately 27:1 to obtain stride frequencies in a useful range, approximately 8-20Hz.

A. Kinematic Transmission Design

The primary difficulty of using a single DC motor to drive a many-legged robot is the kinematic design of a transmission that couples the angular output of the motor to the oscillatory motion of the legs. The Whegs™ family [24], [21], [7] of robots uses a single motor to power hybrid "wheel-legs" through a standard transmission that uses elements like gears and chains. The iSprawl [18] robot uses a single DC motor with an attached slider crank to drive an arrangement of push-pull cables that lengthen and shorten its legs while protraction and retraction are accomplished passively using compliant rotational hips made from a viscoelastic polymer.

Total Mass	23.7gm
Body Size	100 x 45 x 30mm
Maximum speed	1.4 m/s 14 body lengths/s
Maximum stride freq.	20Hz
Motor	Didel MK07-3.3
Battery	Full River 90mAHr lithium polymer
Microcontroller	dsPIC33F
Communications	Bluetooth (Roving Networks rn41 @ 230Kpbs)

TABLE I: Robot physical parameters

The transmission is fabricated using a scaled version of the smart composite microstructures (SCM) process [14]. This method has many advantages: it is inexpensive; its planar nature enables rapid fabrication and assembly; it produces strong, lightweight mechanisms free of friction and backlash; and the compliant mechanisms used in the robotic design can be synthesized and analyzed using standard kinematic approaches.

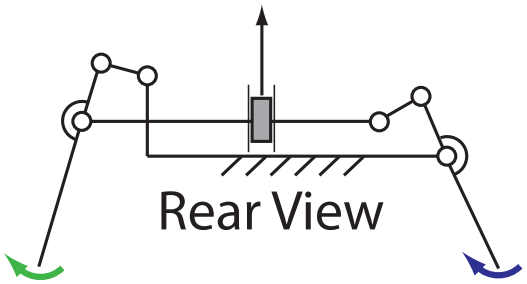

(a) Rear view of the ideal robot kinematics: ab- and adduction of legs from opposite tripods occurs out of phase when the middle member of the linkage is translated vertically.

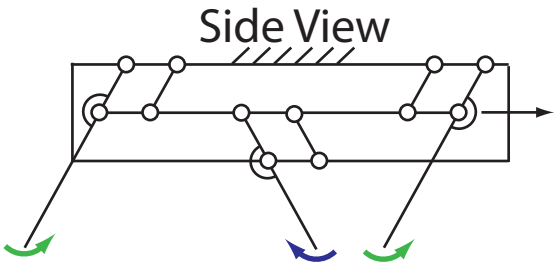

(b) Side view of the ideal robot kinematics: protraction and retraction of the legs is controlled by motion of the middle member in the fore-aft direction. The middle leg moves out of phase with the front and hind legs. Note that in the plane, this configuration appears singular. However, coupling to the degrees of freedom in 2a enables the protraction and retraction of the legs.

Fig. 2: Ideal robot kinematics demonstrating the kinematic coupling enabling an alternating tripod gait. The motor output is aligned with the sagittal plane and a crank provides the vertical and fore-aft motion depicted in each figure.

The robot's kinematics are comprised of two primitive single degree of freedom mechanisms: the slider-crank linkage and the parallel fourbar. Rear and side views of the ideal

kinematics of the robot are shown in Fig. 2. The slider crank linkages enable ab- and ad-duction of the legs, while fourbar linkages enable protraction and retraction.

1) Fourbar Kinematics: The fourbar linkages use a simple parallel geometry and therefore have a transmission ratio of unity. In fact, the driving configuration of the fourbars is an inversion of the standard configuration in which the crank is driven and output is taken from the rocker or coupler link. In the case shown in Fig. 2b, the coupler is driven by the output of the motor and the output of the fourbar is taken at one of the crank links to which a leg is attached. The fourbar was designed for a nominal protraction angle of $\pm 42^\circ$.

By inspection of Fig. 3, the output protraction angle of the leg with respect to the vertical is given by:

$$\theta = \sin^{-1}\left(\frac{h}{r_f}\right) \tag{1}$$

In Eqn. 1, h is due to the motion of the motor crank and is simply given by:

$$h = c\sin\alpha \tag{2}$$

where c is the length of the crank attached to the motor output and α is the crank angle measured with respect to top dead center.

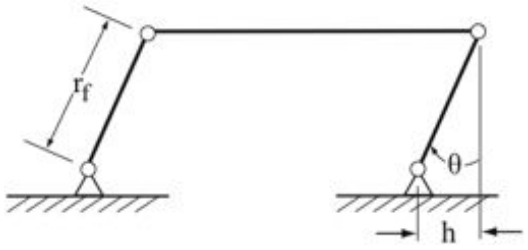

Fig. 3: Schematic of fourbar kinematics

2) Slider Crank Kinematics: In Fig. 2a, the left slider crank is a kinematic inversion of the linkage on the right, and the two legs shown belong to opposite tripods. When the right leg is adducted, the left is abducted and vice versa. Each slider crank was designed to give a nominal abduction angle of 40° measured from the vertical.

To design the slider cranks, we solve the inverse kinematics problem — in our configuration, the slider is the driven element while the output is taken from the crank which functions as a hip (see Fig. 4). The constraint equations are defined as follows:

$$\mathbf{A} = \begin{pmatrix} r_s\cos\psi \\ r_s\sin\psi \end{pmatrix} \tag{3}$$

$$\mathbf{B} = \begin{pmatrix} e \\ s \end{pmatrix} \tag{4}$$

$$(\mathbf{B}-\mathbf{A})^{\mathsf{T}}(\mathbf{B}-\mathbf{A}) = L^2 \tag{5}$$

Note that the link r is shared by both the fourbar linkage and the slider crank. However, in the slider crank formulation, r_s is the projection of r_f onto the transverse plane:

$$r_s = r_f\cos\theta \tag{6}$$

The input from the motor crank drives the slider in the vertical direction giving the relation:

$$s = s_0 - c(1+\sin\alpha) \tag{7}$$

In Eqn. 7 s_0 is the initial value for s. Eqns. 3 - 7 are solved at top and bottom dead center of the crank to determine a value for the length of the coupler L that gives the 40° abduction angle.

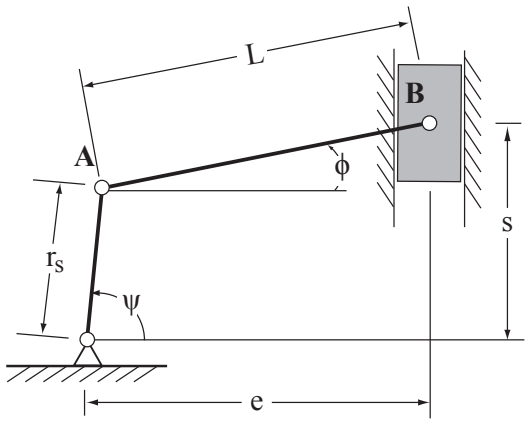

Fig. 4: Schematic of slider crank kinematics

Eqns. 1 - 7 can be combined with the following loop closure equations for the slider cranks [22] to solve the 3D forward kinematics:

$$r_s\cos\psi + L\cos\phi - e = 0 \tag{8}$$

$$r_s\sin\psi + L\sin\phi \pm s = 0 \tag{9}$$

The sign of the s term in Eqn 9 is determined by whether the slider crank is a member of the left or right tripod. Three projections of the solutions to Eqns. 1, 8, and 9 are shown in Fig. 5.

B. Leg Design

We have chosen a semi-circle C shape for the robot's leg similar to the design used on the RHex robot [27]. The leg is manufactured by molding using a stiff polyurethane elastomer with 20% softener by weight (PMC-790 rubber and SO-FLEX softener, Smooth-On, Inc.). The C shape offers three primary advantages: lower vertical stiffness, lateral collapsibility for obstacle climbing, and a rolling instead of point ground contact.

Lower vertical stiffness is obtained by changing the primary loading condition from material compression (as in

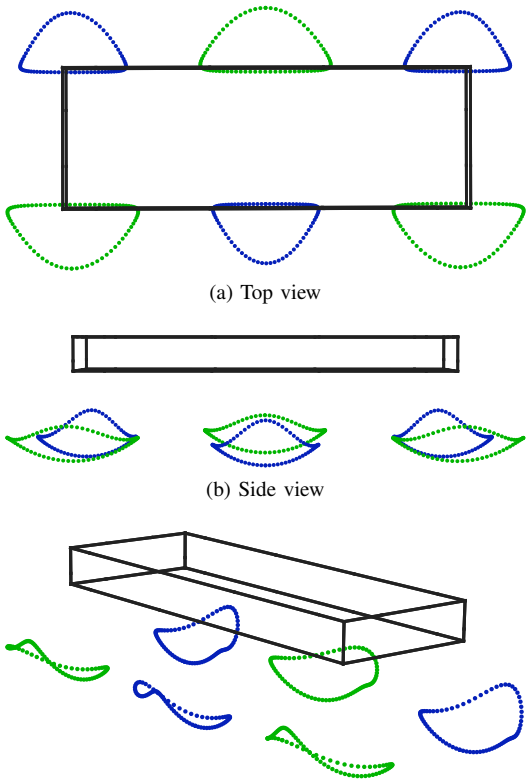

(a) Top view

(b) Side view

(c) Isometric view

Fig. 5: Schematic views of the robot's 3D foot trajectories in a body-centric coordinate frame. Differences in the shape of the foot trajectory for each tripod are a result of a small asymmetry in the kinematic design.

a straight vertical leg) to material flexure. This allows for another actuator to more easily adjust the overall leg stiffness or to change the length of material allowed to deflect in a manner similar to the design in [11].

Collapsibility for obstacle climbing is achieved during forward running, where the open section of the C faces backwards. Upon collision with an object that is taller than the swing clearance height, the C can fold backwards, allowing the leg to continue its forward motion and position some portion of itself on top of the obstacle. During the stride phase, that leg can help pull the robot up and over the object.

The round shape of the C along with its compressibility allows it to form a rolling contact with the ground instead of the isolated point contact associated with a typical straight leg. The rolling behavior resembles a distributed foot, creating less vertical displacement of the center of mass and allowing for smoother overall motion [23].

C. Power, Communication, and Control Hardware

The robot uses the dsPIC33FJ128MC706-based microcontroller board described in [5] for control. Wireless communication is achieved using the Roving Networks rn41 Bluetooth radio interfaced to the PIC microcontroller. Full H-bridge motor control is possible with a custom 2 channel H-bridge motor driver board. However, for this work the robot was driven in a purely open loop, feedforward mode. The motor driver board includes a comparator circuit that enables realtime measurement of the motor back EMF voltage. The analog to digital converter on the PIC is configured to sample during the off portion of the motor pulse width modulation signal.

III. Models for Dynamic Turning in Hexapods

In [16], Jindrich and Full argue that all legs of a cockroach can contribute to turning maneuvers. Inspired by measurements of leg kinematics and ground reaction forces, they devise a simple planar model to describe turning. Then they propose a metric for leg turning effectiveness that represents the ability of the leg to generate forces perpendicular to the heading vector and apply the metric to the model. While the front leg on the outside of the turn was found to produce the most force perpendicular to the heading, the outside middle leg was also found to produce forces that rotate the cockroach appropriately. However, their model requires the middle leg to produce additional force parallel to the heading in order to compensate for the resulting change in body orientation relative to the heading.

In an effort to further explore the dynamics of turning, Proctor and Holmes demonstrated that the lateral leg spring (LLS) model [28], a low-dimensional conservative model of locomotion in the plane, is capable of producing dynamic turning [26]. By momentarily changing leg stiffness and touchdown angle, they demonstrate that translational kinetic energy can be temporarily exchanged for rotational kinetic energy, thus inducing a turn. In particular, they predict significant turning rates for increases in spring constant of $\approx$ 50% and shifts in the location of the center of pressure (CoP) of less than $\approx$ 10% of total body length ; results from the simulation investigation are reprinted in Fig. 6.

While Proctor and Holmes' model seems to support Jindrich and Full's assertion that turning can be achieved via small adjustments to a straight running gait, one drawback is that LLS parameters cannot be directly mapped to the design parameters of a physical six-legged robot. For example, LLS collapses a tripod of three legs into a single "effective" leg, making it impossible, as Jindrich and Full did, to differentiate between an outside front leg and an outside middle leg since those two legs belong to different tripods (but are located on the same side of the body).

For this reason, we attempt to induce turning of a real physical robotic system by directly adjusting leg stiffness and characterizing the turning behavior that results. By demonstrating stiffness-mediated turning in a hexapedal robot, we aim to increase understanding of the role leg stiffness plays in dynamic maneuvers and propose a bio-inspired approach to motion control suitable for small, underactuated robots.

IV. Experimental Setup

Experiments were recorded with high-speed video from an overhead camera (250fps, 8bit grayscale, 1280×1024px, AOS Technologies). The frame sequences were downloaded to a desktop computer in uncompressed RAW format and

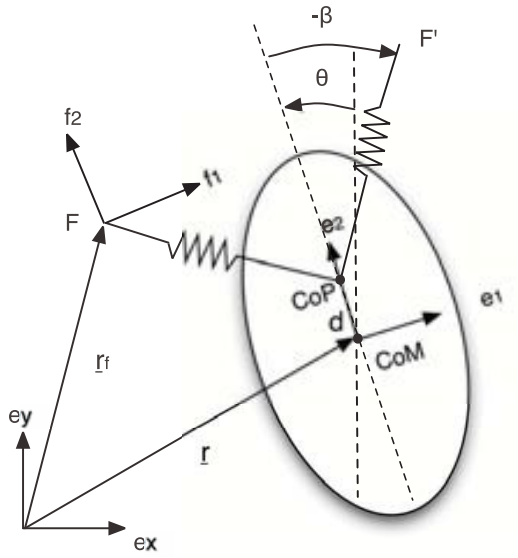

(a) From [26]: A schematic of the lateral leg spring (LLS) model and relevant physical parameters.

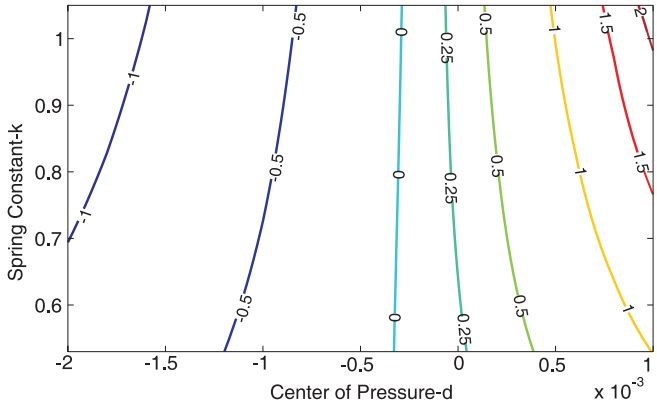

(b) From [26]: A contour map of turning angle in radians over 3 strides as a function of the model's leg stiffness k and center-of-pressure (CoP) offset from the center-of-mass.

Fig. 6: From [26]: The lateral leg spring (LLS) model and turning prediction.

processed with the Python programming language using OpenCV [1] and the SciPy package [2].

A. Substrate

A 1m×1m sheet of cork was fixed to the laboratory floor, and experiments were performed entirely on the cork's surface. Cork increases foot traction, which was deemed desirable for these experiments. However, cork also introduces compliance into the ground contact, conceivably confounding empirical results. Based on the experimentally determined value of the Young's modulus of cork reported in [12], 20 MPa, we can estimate an approximate stiffness for the cork substrate. Assuming a dynamic load of twice the full weight of the robot supported by a single leg contacting over an area of one mm^2, the approximate linear stiffness of the cork is 6500N/m. Since this is more than two orders of magnitude larger than the typical leg compliance, we consider its effect negligible in the experiments.

B. Leg Stiffness

For the turning experiments we adjust leg stiffness by replacing the middle leg fabricated from soft polyurethane rubber containing 20% plasticizer ($E \approx 10.7$MPa) by weight with a leg of the same geometry fabricated from the same polyurethane without plasticizer ($E \approx 24.5$ MPa). Flexural moduli for the two materials were determined experimentally using a standard end-loaded linear beam test. Experimentally measured dynamic linear stiffnesses for both soft and stiff legs are plotted in Fig. 11b. The nominal leg stiffness was tuned manually to yield qualitatively smooth and fast open loop forward running.

C. Camera Calibration

1) Intrinsics: Before conducting experiments with the robot, multiple image sequences were recorded of a planar calibration chessboard (7×8 squares, 29mm per side) held in different poses covering the image plane. We model the camera as a pinhole with fourth order radial lens distortion and zero tangential skew. The intrinsic parameters were estimated by running the software described in [20] on our calibration sequences.

2) 2D Extrinsics: To support estimation of the kinematic state of the running robot, we estimated the equation of the plane containing the cork surface in the camera's reference frame. To simplify the estimation, we restricted the chessboard to slide across the cork surface for one sequence of calibration images, eliminating out-of-plane rotation and translation. Adding this constraint allowed us to simultaneously estimate the cork plane together with the three-dimensional pose of the chessboard on the surface in each video frame using nonlinear least-squares. This approach was superior to fitting a plane to the 3D point cloud obtained by estimating the chessboard's pose independently in each sample.

3) 3D Extrinsics: To extract three-dimensional trajectory data, we use a single camera viewing a scene from two perspectives; one view is direct, and the other passes through a slanted mirror. We jointly estimate the intrinsic camera parameters and extrinsic rigid transformation between the stereo pair using the software described in [20].

D. Tracking Geometry

Retro-reflective spheres (Mocap Solutions, CA) were affixed to laminated strips of balsa wood glued to the robot's chassis. Aligning a pair of HMI lights (Super-Sun Gun 200W, Frezzolini) with the camera axis enabled segmentation of these spheres in videos via simple thresholding. The three-dimensional geometry of the spheres affixed to the robot was estimated using the two-camera setup described in Section IV-C.3 using a video of the robot translating through the field of view. The 3D location of each reflective sphere was estimated independently in each sample, then these observations were rigidly transformed to align about the origin. We then averaged these 3D locations to obtain an estimate of the geometry.

E. State Estimation

Using the calibrated cork surface and robot tracking geometry from Sections IV-C.2 and IV-D, it is possible to estimate the robot's rotations and planar position using pixel observations of the reflective spheres from a single overhead camera. We perform state estimation using an Unscented Kalman Filter (UKF) whose state is comprised of Euler rotations $(\theta_x, \theta_y, \theta_z)$ about the x, y, and z axes and planar position (x, y) (for theoretical details about the UKF, refer to [17]; for implementation details, see [30]).

V. Results

A. Running Speed

In both straight ahead running and turning, the top speed of the robot was estimated to be 1.4 m/s or 14 body lengths/s. Fig. 7 shows the robot's running speed as a function of stride frequency for all trials including turning and straight running.

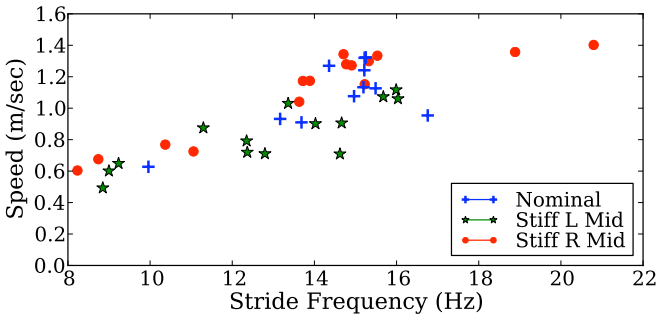

Fig. 7: Forward speed vs. stride frequency

B. Turning by Stiffness Control

Results from the study of turning in cockroaches suggest that all legs have the potential to contribute to dynamic turning. Though in [16] the front legs were posited to induce turning most effectively, we found empirically that stiffening a middle leg gave rise to turning more consistently.

With a stiffer middle leg in place, the robot was run over a flat cork surface at a variety of speeds. The results from the turning experiments are shown in Figs. 8 and 9. Fig. 8 demonstrates that by stiffening the middle leg, we are able to consistently achieve turning in either direction. Qualitative examination of the figure, however, reveals that the robot turns more smoothly to the left than to the right, a fact that may be explained by small kinematic asymmetries in the robot's gait. Likewise, Fig. 9 shows that the maximum turning rate is relatively insensitive to stride frequency while there appears to be a wide scatter of turning rates possibly due to as-yet unmodeled frequency-dependent dynamics. Data for the left turn show a mean turning rate of approximately 75 degrees per second, while the mean turning rate for right turns is approximately 50 degrees per second with significantly more variation in the data.

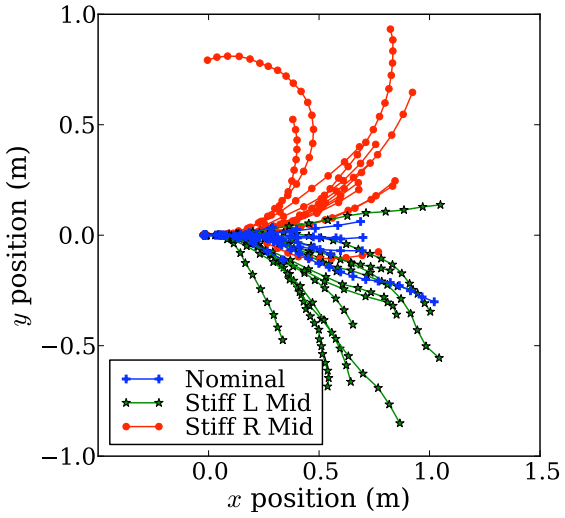

Fig. 8: Summary data from all turning and straight running trials at 8-20Hz stride frequencies.

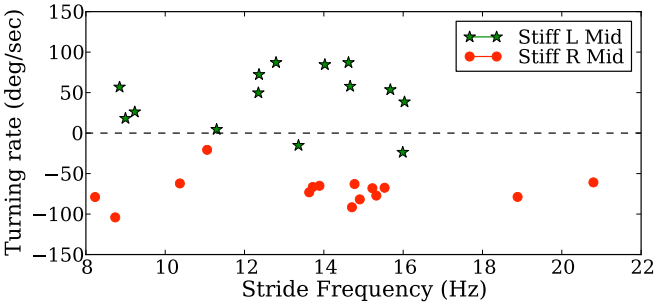

Fig. 9: Turning rate vs. stride frequency

VI. Discussion

We demonstrated turning and rapid running in a small underactuated legged robot. Simply by stiffening the middle leg on the opposite side of the desired turn direction, we induced turning at rates of roughly 50 degrees per second to the right and 75 degrees per second to the left. The turning rate does not appear to vary smoothly with respect to stride frequency (see Fig. 9) even when the robot exhibits a periodic trajectory. However, we believe further kinematic refinements and feedback control can be employed to compensate for these irregularities.

Based on simple planar biological models for turning in hexapods, we anticipated that stiffening the middle leg would initiate turning. Though the model in [16] predicted that increasing the front leg stiffness would be most effective for initiating turning, the middle leg gave better results for our robot. This inconsistency may arise simply due to differences in gait kinematics and scale between our robot and the cockroaches studied in [16]. In particular, our robot's limbs are significantly less sprawled than a cockroach's, complicating the mapping between our robot's physical design parameters and the lumped model parameters found in [16] or [26].

At specific stride frequencies, we observed rapid dynamic turns in which the robot turned $\approx 90^\circ$ over roughly 5 strides; see Fig. 10 for data from an illustrative trial. Of note is the fact that large instabilities in the robot's roll (rotation

about the major body axis in the horizontal plane) and pitch (rotation about the body minor axis) correlate with the turns, settling out immediately following the execution of the maneuver. We believe this is an exciting result deserving of more study; the ability of a legged robot to reliably execute such sharp turns would lead to extremely rapid navigation. It is also worth noting that this maneuver appears to depend crucially on out-of-plane rotational dynamics, potentially limiting the ability of planar models to explain the behavior.

Our demonstration of consistent turning via modulation of leg stiffness has implications for biomechanics research. Since it is easy to adjust leg stiffness on our robot by simply replacing the leg, the platform can support systematic studies of the parametric dependence of maneuverability. We have already provided preliminary experimental validation for the turning predictions from simple models like LLS. We aim to extend this result by carefully characterizing the connection between the lumped-element parameters in (for example) LLS and the physical robot.

VII. Future Work

To actively initiate turning, we propose adjusting the stiffness of the middle leg on each side using shape memory alloy wire attached to the leg as shown in the CAD drawing in Fig. 11a. The wire is 75 μm diameter Flexinol (Dynalloy, Tustin, California, USA) that is run from the hip down along the outside of the C, then turned around on a piece of plastic embedded in the leg material before running up along the C back to the hip, where it is connected to control electronics. Actuation of the SMA wire increases its modulus and decreases its length. The result is a significant increase in the area moment of inertia and, thus, the flexural rigidity of the whole leg.

To verify that our design can achieve the same increase in stiffness as fabricating the legs without plasticizer, we tested the dynamic stiffness of a "soft" leg with an actuator attached using a muscle lever (300C, Aurora Scientific) to apply varying loads at frequencies in the range of the running frequencies the robot is capable of. The leg was tested in both actuated and unactuated states with a simple benchtop DC power supply providing the current required to heat the SMA. Fig. 11b shows that at applied dynamic loads between 50mN and 80mN, the actuated leg is capable of matching or nearly matching the stiffness of the harder polyurethane. We are encouraged by this result as it demonstrates a clear integration path for active leg stiffness modulation.

Integration of the active leg will require a control strategy for turning. Given that SMA is easiest to operate using simple on-off control, the leg will initially be used simply to initiate turning (without attempting to modulate turning radius) with a control bandwidth of approximately 1 Hz. And, because operation is intermittent, the relative inefficiency of SMA is less of a concern than it would be if it were employed as a power actuator.

It is important to distinguish a robot's (numerous) design parameters from the (few) lumped parameters in a low-order

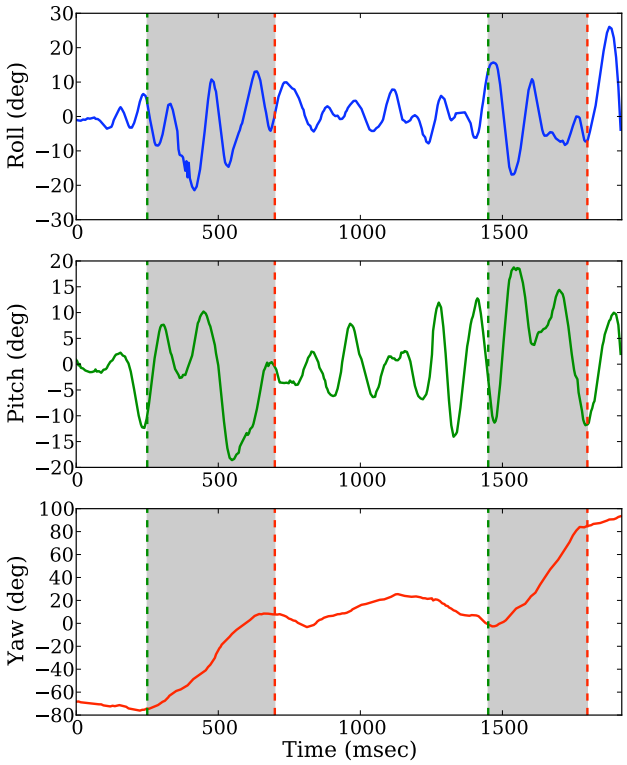

(a) Robot orientation during dynamic turns. Note increases in roll and pitch magnitudes corresponding to sudden changes in yaw.

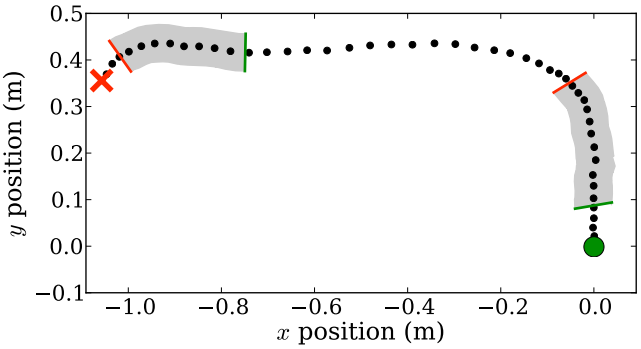

(b) Position data for the robot during dynamic turns. The time interval between markers is 40ms and the stride frequency is approximately 13Hz. Green circle indicates start of trial; red "×" indicates end.

Fig. 10: Rotation and position traces showing the robot executing two rapid dynamic turns. Grey regions encompass corresponding time intervals in each figure to facilitate comparison.

abstraction of that robot's dynamics. For such an abstraction to have any predictive power, there must be a well-behaved map from the physical parameters to those of the model. To rigorously test a model's prediction, one must characterize that map for the physical system of interest. Thus for us to rigorously claim that we have empirically validated a prediction of the lateral leg-spring model, we must perform parameter identification between LLS and our physical robot to characterize the map between, e.g., the robot's dynamic leg stiffness in Fig. 11b and the stiffness parameter in LLS [26]. We are actively studying this parameter identification problem.

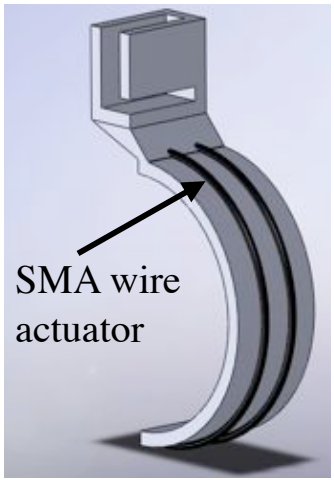

(a) A CAD depiction of the compliant semi-circular leg with shape memory alloy wires running along the outside of the leg.

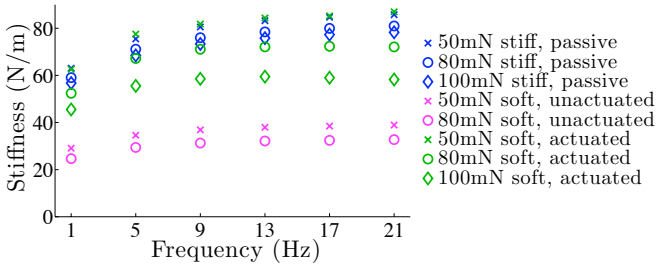

(b) Experimental measurements of dynamic leg stiffness comparing a passive, "stiff" leg to a "soft" leg with an integrated shape memory alloy (SMA) wire actuator tested at applied dynamic loads of 50mN, 80mN, and 100mN.

Fig. 11: Design and initial experimental results for leg with actively controlled stiffness.

VIII. Acknowledgements

We thank Tom Libby for invaluable assistance with data collection and analysis and the UC Berkeley Center for Interdisciplinary Bio-inspiration in Education and Research (CiBER) for the use of the muscle lever setup for characterizing leg stiffness.

References

[1] [Online]. Available: http://opencvlibrary.sourceforge.net
[2] [Online]. Available: http://www.scipy.org
[3] S. Avadhanula, "The design and fabrication of the MFI thorax based on optimal dynamics," Master's thesis, University of California, Berkeley, 2001.
[4] S. Bergbreiter, "Design of an autonomous jumping robot," in *IEEE Int. Conf. on Robotics and Automation*, Rome, Italy, April 2007.
[5] F. G. Bermudez and R. S. Fearing, "Optical flow on a flapping wing robot," in *Intl Conf on Intelligent Robots and Systems*, St. Louis, MO, 2009, pp. 5027–5032.
[6] P. Birkmeyer, K. Peterson, and R. S. Fearing, "Dash: A dynamic 16g hexapedal robot," in *IEEE Int. Conf. on Intelligent Robots and Systems*, 2009.
[7] A. Boxerbaum, J. Oro, G. Peterson, and R. Quinn, "The latest generation Whegs^{TM}; robot features a passive-compliant body joint," sept. 2008, pp. 1636 –1641.
[8] J. G. Cham, S. A. Bailey, J. E. Clark, R. J. Full, and M. R. Cutkosky, "Fast and robust: Hexapedal robots via shape deposition manufacturing," *The International Journal of Robotics Research*, vol. 21, no. 10-11, pp. 869–882, 2002.
[9] F. Delcomyn, "The locomotion of the cockroach periplaneta americana," *J Exp Biol*, vol. 54, no. 2, pp. 443–452, 1971.
[10] M. H. Dickinson, C. T. Farley, R. J. Full, M. A. Koehl, R. Kram, and S. Lehman, "How animals move: An integrative view," *Science*, vol. 288, no. 5463, pp. 100–106, 2000.
[11] K. Galloway, J. Clark, and D. Koditschek, "Design of a tunable stiffness composite leg for dynamic locomotion," in *ASME IDETC/CIE*, 2009.
[12] L. J. Gibson, K. E. Easterling, and M. F. Ashby, "The structure and mechanics of cork," *Proceedings of the Royal Society of London. Series A, Mathematical and Physical Sciences*, vol. 377, no. 1769, pp. 99–117, 1981. [Online]. Available: http://www.jstor.org/stable/2397034
[13] J. K. Hodgins and M. H. Raibert, "Biped Gymnastics," *The International Journal of Robotics Research*, vol. 9, no. 2, pp. 115–128, 1990.
[14] A. M. Hoover and R. S. Fearing, "Fast scale prototyping for folded millirobots," in *IEEE Int. Conf. on Robotics and Automation*, Pasadena, CA, 2008.
[15] D. L. Jindrich and R. J. Full, "Dynamic stabilization of rapid hexapedal locomotion," *J Exp Biol*, vol. 205, no. 18, pp. 2803–2823, 2002.
[16] D. Jindrich and R. Full, "Many-legged maneuverability: dynamics of turning in hexapods," *J Exp Biol*, vol. 202, no. 12, pp. 1603–1623, 1999.
[17] S. J. Julier and J. K. Uhlmann, "New extension of the Kalman filter to nonlinear systems," I. Kadar, Ed., vol. 3068, no. 1. SPIE, 1997, pp. 182–193.
[18] S. Kim, J. E. Clark, and M. R. Cutkosky, "iSprawl: Design and tuning for high-speed autonomous open-loop running," *The International Journal of Robotics Research*, vol. 25, no. 9, pp. 903–912, 2006.
[19] M. Kovac, M. Schlegel, J.-C. Zufferey, and D. Floreano, "Steerable miniature jumping robot," *Autonomous Robots*, vol. 28, no. 3, pp. 295–306, 2010.
[20] G. Kurillo, Z. Li, and R. Bajcsy, "Framework for hierarchical calibration of multiple-camera systems for teleimmersion," in *IMMERSCOM*. ICST, 2009, p. 1.
[21] B. Lambrecht, A. Horchler, and R. Quinn, "A small, insect-inspired robot that runs and jumps," in *IEEE Int. Conf. on Robotics and Automation*, Barcelona, Spain, 2005, pp. 1240–1245.
[22] J. M. McCarthy, *Geometric Design of Linkages*, 1st ed., J. E. Marsden, L. Sirovich, and S. Wiggins, Eds. Springer, 2000.
[23] E. Moore, "Leg design and stair climbing control for the rhex robotic hexapod," Master's thesis, McGill University, 2002.
[24] J. M. Morrey, B. Lambrecht, A. D. Horchler, R. E. Ritzmann, and R. D. Quinn, "Highly mobile and robust small quadruped robots," in *Intl Conf on Intelligent Robots and Systems*, vol. 1, 2003, pp. 82–87.
[25] R. Playter, "Passive dynamics in the control of gymnastic maneuvers," Ph.D. dissertation, Massachusetts Institute of Technology, 1995.
[26] J. Proctor and P. Holmes, "Steering by transient destabilization in piecewise-holonomic models of legged locomotion," *Regular and Chaotic Dynamics*, vol. 13, no. 4, pp. 267–282, 2008.
[27] U. Saranli, M. Buehler, and D. E. Koditschek, "RHex: A simple and highly mobile hexapod robot," *The Int. J. of Robotics Research*, vol. 20, no. 7, pp. 616–631, 2001.
[28] J. Schmitt and P. Holmes, "Mechanical models for insect locomotion: dynamics and stability in the horizontal plane I. theory," *Biol. Cyber.*, vol. 83, no. 6, pp. 501–515, 2000.
[29] ——, "Mechanical models for insect locomotion: dynamics and stability in the horizontal plane –II. application," *Biological Cybernetics*, vol. 83, no. 6, pp. 517–527, 11 2000.
[30] A. Spence, S. Revzen, J. Seipel, C. Mullens, and R. Full, "Insects running on elastic surfaces," *Journal of Experimental Biology*, In preparation.
[31] S. Sponberg and R. J. Full, "Neuromechanical response of musculoskeletal structures in cockroaches during rapid running on rough terrain," *J Exp Biol*, vol. 211, no. 3, pp. 433–446, 2008. [Online]. Available: http://jeb.biologists.org/cgi/content/abstract/211/3/433
[32] E. E. Steltz, "Redesign of the micromechanical flying insect in a power density context," Ph.D. dissertation, University of California, Berkeley, 2008.
[33] R. J. Wood, S. Avadhanula, R. Sahai, E. Steltz, and R. S. Fearing, "Microrobot design using fiber reinforced composites," *J. Mech. Design*, vol. 130, no. 5, May 2008.